



HAL
open science

Seismic evidence of fluid migration in northeastern Japan after the 2011 Tohoku-Oki earthquake

Qingyu Wang, Michel Campillo, Florent Brenguier, Albanne Lecointre,
Tetsuya Takeda, Keisuke Yoshida

► **To cite this version:**

Qingyu Wang, Michel Campillo, Florent Brenguier, Albanne Lecointre, Tetsuya Takeda, et al.. Seismic evidence of fluid migration in northeastern Japan after the 2011 Tohoku-Oki earthquake. *Earth and Planetary Science Letters*, 2021, 563, pp.116894. 10.1016/j.epsl.2021.116894 . hal-03180473

HAL Id: hal-03180473

<https://hal.univ-grenoble-alpes.fr/hal-03180473>

Submitted on 25 Mar 2021

HAL is a multi-disciplinary open access archive for the deposit and dissemination of scientific research documents, whether they are published or not. The documents may come from teaching and research institutions in France or abroad, or from public or private research centers.

L'archive ouverte pluridisciplinaire **HAL**, est destinée au dépôt et à la diffusion de documents scientifiques de niveau recherche, publiés ou non, émanant des établissements d'enseignement et de recherche français ou étrangers, des laboratoires publics ou privés.

1 **Seismic evidence of fluid migration in northeastern Japan after the 2011 Tohoku-Oki**
2 **earthquake**

3

4 Qing-Yu Wang^{1,2}, Michel Campillo¹, Florent Brenguier¹, Albanne Lecointre¹, Tetsuya
5 Takeda², Keisuke Yoshida³

6 1. Department of Earth, Atmospheric and Planetary Sciences, Massachusetts Institute of
7 Technology, Cambridge, USA.

8 2. Université Grenoble Alpes, CNRS, ISTERre, Grenoble, France

9 3. National Research Institute for Earth Science and Disaster Resilience, Japan

10 4. Department of Geophysics, Graduate School of Science, Tohoku University, Japan

11

12 ***Corresponding author : Qing-Yu Wang**

13 Address : ISTERre, 1381 Rue de la Piscine, Saint Martin d'Hères, 38400, France

14 Email : qingyuwa@mit.edu

15 Tel : +33 (0)6 01 12 21 94

16 **Abstract**

17

18 We use ambient-noise-based seismic monitoring to detect an anomalous seismic velocity
19 decrease ($\sim 0.01\%$) widely distributed in Honshu that arose about 1 year after the 2011 M_w
20 9.0 Tohoku-Oki earthquake. The anomaly is located along the central quaternary volcanic
21 axis, and it suggests that the changes are related to volcanic processes. After correction for
22 possible external environmental forcing-related velocity changes, the anomaly in the seismic
23 velocity remains, which implies that it is associated with some internal physical process. We
24 show a general strong positive correlation between the seismic velocity changes and the
25 intensity of ground motion derived from the daily cumulative seismic moment. However, the
26 lack of correlation during the anomaly itself reveals that this reduction is not directly caused
27 by earthquake shaking. Tiltmeter low-pass observations show temporal variations that are
28 correlated with the velocity changes. These observations strengthen the hypothesis of actual
29 physical deformation. A previously reported decrease in fault strength ($\sim 10\%$) for the same
30 period as the velocity anomaly further supports a physical property change in the upper crust.
31 We also note a simultaneous increase in activity of low-frequency events in the volcanic area,
32 which suggests an increase in pore pressure in the upper crust. We propose that the observed
33 anomalous seismic velocity decrease in early 2012 is due to an increase in pore pressure
34 induced by an upward fluid migration, which at the same time triggered the increase in fluid-
35 driven swarm seismicity and low-frequency events. We recall the depth-dependent seismic
36 velocity changes in Honshu and derive an average diffusion of $1 \text{ m}^2/\text{s}$ over around 11 months
37 after the Tohoku-Oki earthquake.

38

39 **Keywords:**

40 Seismic velocity drop anomaly; Fluid migration; Low frequency earthquakes; Tiltmeter

41 observation; Pore pressure; Fault strength.

42

43 **1. Introduction**

44

45 Ambient noise monitoring allows changes in seismic wave velocities related to large
46 earthquakes to be followed. The main observation is the rapid coseismic velocity drop at
47 shallow depths under the impact of strong ground motion caused by earthquakes, such as: the
48 2004 M_w 6.0 Parkfield (Brenuier et al. 2008) and 2008 M_w 7.9 Wenchuan (Chen et al., 2010;
49 Froment et al., 2013) earthquakes; the 2009 M_w 6.3 L'Aquila earthquake (Poli et al., 2020);
50 the 2011 M_w 9.0 Tohoku-Oki earthquake (Brenuier et al., 2014; Sawazaki et al., 2015;
51 Wang et al., 2019); and the 2014 M_w 6.0 South Napa earthquake (Taira et al., 2015).
52 Shallow-depth changes are also due to seasonal velocity changes caused by environmental
53 forces (Hobiger et al., 2012; Wang et al., 2017; Poli et al., 2020). Deeper static strain (Wang
54 et al., 2019) and strong aftershocks (Sawazaki et al., 2015) can also cause distinctive changes
55 in seismic wave velocities, as seen for the 2011 Tohoku-Oki earthquake.

56

57 In this study, we use data from the short-period seismic network Hi-net (Okada et al., 2004;
58 Obara et al., 2005) that provides even cover of the island of Honshu. We focus on the
59 response of the shallow crust in the frequency range from 0.15 Hz to 0.90 Hz, which is
60 basically down to a depth of about 5 km, according to the surface wave sensitivities of the
61 ambient seismic noise. A large coseismic drop of velocity occurred coincident with the
62 Tohoku-Oki earthquake of March 11, 2011. After a short relaxation time, the velocity
63 reached a minimum with the significant aftershock of M_w 7.2 on April 7, 2011, near the east
64 coast of Honshu. Then the velocity started to gradually increase following a roughly
65 logarithmic recovery, in a way similar to that observed after several events with periods <10 s
66 (Brenuier et al., 2008; Wegler et al., 2009; Hobiger et al., 2012; Taira et al., 2015). In the
67 case of the Tohoku-Oki earthquake, about 11 months after the earthquake, there was a

68 secondary episode of decreased velocity that occurred for a large number of the stations in
69 Honshu. We outline this secondary episode of decrease in velocity as the seismic evidence of
70 fluid migration after the Tohoku-Oki earthquake.

71

72 The velocity changes averaged over northern Honshu show a late anomalous seismic velocity
73 drop. The spatial distribution of the amplitudes of these velocity drops correlates with the
74 central volcanic axis, where is in agreement with the volcanic subsidence of 5 - 15 cm just
75 after the Tohoku-Oki earthquake reported by Takada & Fukushima (2013). They discussed
76 the possible origins with two major hypothesis of hot and weak material, water release. In
77 this paper. We first correct the possible environmental effects with different experiments and
78 confirm the existence of this velocity anomaly in this special location. Seismic intensity
79 envelopes based on the seismicity can perfectly explain the global changes in seismic velocity
80 even some quick and small velocity variations, especially for the time period before the
81 Tohoku-Oki earthquake. Nevertheless, there is a lack of evidence to correlate this anomaly in
82 2012 to the intensity envelop. By comparing borehole tiltmeter recordings from the same site,
83 we identify a similar anomaly for the tiltmeter low-pass time series, with ground tilt of
84 several microradians. Other observations, such as the synchronous increased rate of low-
85 frequency earthquakes (LFEs) and the simultaneous decrease in fault strength (Yoshida et al.,
86 2016) around the volcanic area, contribute further arguments on tracing the common physical
87 origins. With comprehensive observations and discussions, we speculate that these regional
88 velocity decreases are likely to be directly related to the activities of underground fluids. The
89 upward fluid migration through the crust led to the increase of the pore pressure and further
90 produced this seismic velocity decrease anomaly. Based on all the depth-dependent
91 observations (Want et al., 2019), we derive an average diffusion through the crust of $\sim 1\text{m}^2/\text{s}$
92 over around 11 months after the mainshock in Honshu.

93

94 **2. Data and observations**

95

96 We use the data for the continuous daily seismic velocity changes measured using noise-
97 based monitoring in the frequency range of 0.15 Hz to 0.90 Hz (Wang et al., 2017), and focus
98 on an interpretation of the seismic decrease anomaly observed in early 2012 in Honshu.
99 Figure 1a shows the 236 Hi-net stations that provide the data used in this study. We get the
100 seismic velocity changes at each station using the doublet and inversion method (Brennguier et
101 al., 2014). More details of the data processing procedures and methods applied are given in
102 Wang et al. (2017).

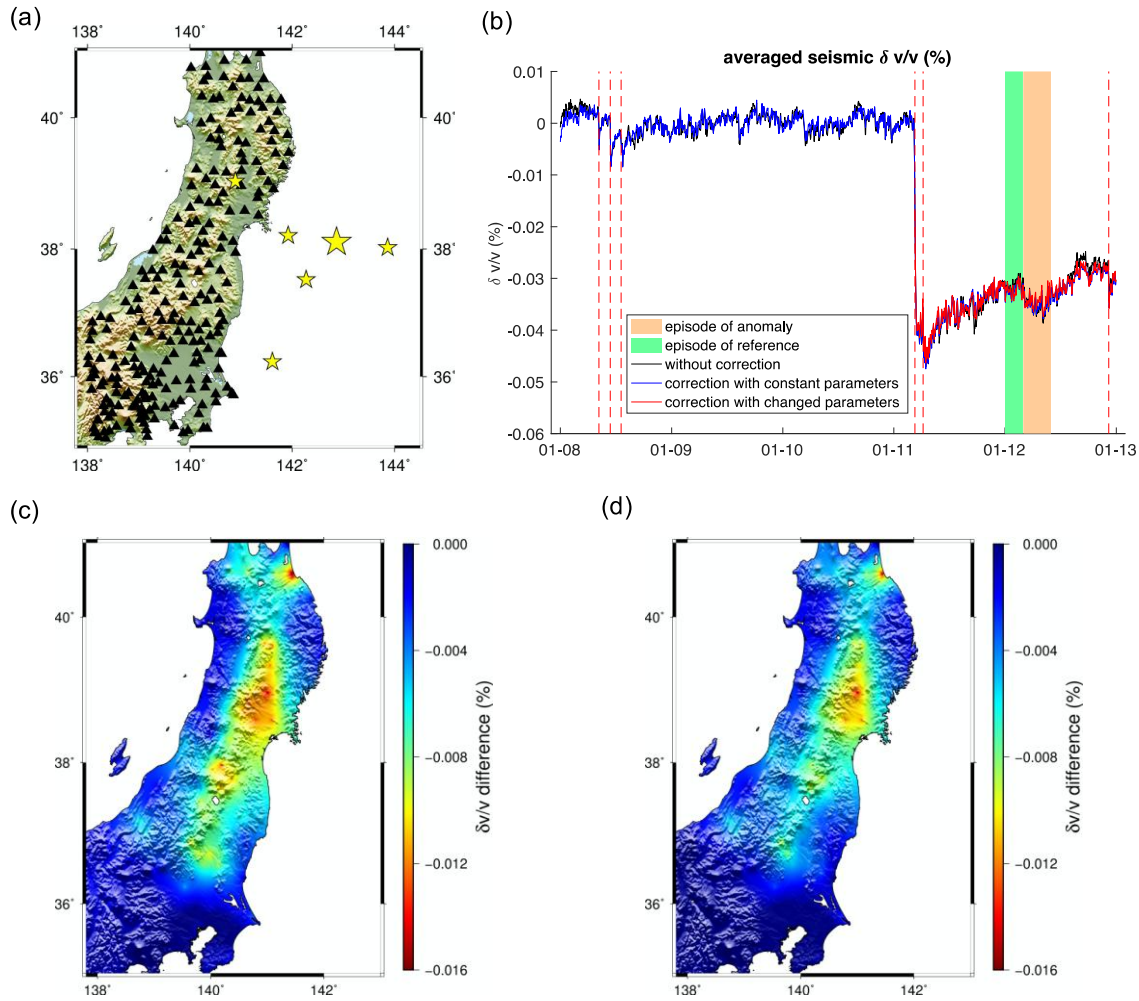
103

104 When only the Rayleigh wave sensitivity kernels are considered, the velocity measurements
105 in the studied frequency band mainly characterize the changes in the physical properties
106 within the 5 km of the upper crust (Obermann et al., 2018; Wang et al., 2019). Using the time
107 series of the velocity changes (Figure 1b) averaged over all of stations in Figure 1a, it is
108 possible to identify some rapid velocity drops that are coincident with some large earthquakes.
109 After checking all the earthquakes with magnitude larger than six, we are able to easily
110 identify velocity decreases related to six earthquakes larger than magnitude around seven.
111 The dates of earthquakes are indicated by the red vertical dashed lines in Figure 1b. The six
112 large earthquakes from the JMA catalog are separately: M_w 7.0 on May 8, 2008; M_w 7.2 on
113 June 14, 2008; M_w 6.9 on July 19, 2008; M_w 9.0 on March 11, 2011; M_w 7.2 on April 7, 2011;
114 and M_w 7.2 on December 7, 2012. Among these earthquakes, the M_w 9.0 Tohoku-Oki
115 earthquake on March 11, 2011 produced the largest velocity drop. After the Tohoku-Oki
116 earthquake, the velocity then increased due a relaxation process that has been reported
117 previously in a number of studies (Brennguier et al., 2014; Hobiger et al., 2012; Wang et al.,

118 2019). The minimum velocity reached is actually coincident with its significant aftershock of

119 M_w 7.3 on April 7, 2011.

120



121

122 **Figure 1.** (a) Map of the study area. Black triangles, the 236 Hi-net stations for the data used in this study;
 123 yellow stars, epicenters of the earthquakes considered, are separately the M_w 7.0, 08-May-2008 (36.24°N
 124 141.61°E), the M_w 7.2, 14-Jun-2008 (39.04°N 140.89°E), the M_w 6.9, 19-Jul-2008 (37.52°N 142.27°E), the M_w
 125 9.0, 11-Mar-2011 (38.11°N 142.87°E), the M_w 7.2, 07-Apr-2011 (38.21°N 141.92°E), and the M_w 7.2 07-Dec-
 126 2012 (38.02°N 143.87°E). (b) Time series of averaged seismic velocity changes. Black curve represents the
 127 time series for the seismic velocity changes averaged over all of the 236 Hi-net stations in (a). Blue curve and
 128 red curve are corrected velocity changes with constant parameters and changed parameters, respectively. Red
 129 vertical dashed lines, dates of the earthquakes (a; yellow stars); green shaded time period, reference episode
 130 before the anomaly; orange shaded time period, anomaly episode. (c, d) Maps showing the differences in the
 131 changes in seismic velocities between the anomaly episode and the reference episode in (b), without correction
 132 (c) and after removal of the environmental effects (d).

133

134 Aside from the earthquake-related velocity changes, there is an anomalous seismic velocity
135 decrease of $\sim 0.01\%$ in early 2012 (highlighted by the orange band, Figure 1b). The amplitude
136 of this anomaly is comparable to the abrupt decreases associated with the indicated
137 magnitude ~ 7.0 earthquakes (e.g., Iwate-Miyagi Nairiku inland earthquake on June 14, 2008).
138 In Figure 1b, the black time series shows the raw monitoring result without any correction for
139 the external environmental effects. The differences between the variations of the seismic
140 velocities averaged for the two time periods indicated by the green shaded band (from
141 January 1, 2012 to February 29, 2012) and the orange band (from March 1, 2012 to May 31,
142 2012) in Figure 1b are then calculated. The map of this difference is shown in Figure 1c, and
143 this illustrates the correspondence between the velocity drop and the central volcanic zone.
144 Therefore, we consider this velocity anomaly to be located in the upper crust of the volcanic
145 area, which is believed to have high susceptibility of velocity changes to stress perturbations
146 (Brenquier et al., 2014). This specific distribution is a good indication that the drop is not an
147 artifact of the measurements, as such an effect of a change in the nature of the noise would
148 not be expected to correlate with the geological structure.

149

150 The overall changes (Figure 1b, black curve) in the study area are stable in time, other than
151 the occurrence of a significant earthquake or this anomaly in early 2012. This velocity change
152 anomaly does not show the characteristics of seasonal effects. Wang et al. (2017) show that
153 seasonal variations on the east side of Honshu Island are weak. Nevertheless, it is recognized
154 that seismic wave velocities can be strongly affected by many surrounding environmental
155 perturbations, e.g., groundwater level changes and rainfall can decrease seismic velocities by
156 0.01% to 0.1% through increased pore pressure (Sens-Schönfelder & Wegler, 2006; Meier et
157 al., 2010; Hillers et al., 2014; Wang et al., 2017). Also, some direct loading associated with
158 snowfall, precipitation, and sea-surface height changes can affect the seismic wave velocities

159 (Wang et al., 2017; Donaldson et al., 2019). Further, in the shallow layer, thermoelastic stress
160 and atmospheric pressure can modulate the seismic wave velocities on an annual cycle
161 (Meier et al., 2010; Richter et al., 2014; Hillers et al., 2015). Therefore, we first investigate
162 whether the environmental factors represent the origin of this anomaly. Wang et al. (2017)
163 propose a scheme of correction for these effects based on the actual observations of
164 precipitation, snow load, and sea-surface height variations. The correction is empirically
165 parameterized from the observations between 2009 and 2010, a period during which no major
166 earthquakes occurred in this region.

167

168 The first operation here is to apply the linear model of Wang et al. (2017) to correct the
169 possible changes from combined effects of hydro-meteorological factors. The parameters of
170 the correction at each station are established using the period from 2009 to 2010, when no
171 known major seismic events occurred. The extension of this correction to the period of 2011
172 to 2012 is carried out under the assumption that the changes in the seismic velocity due to the
173 external forcings after the Tohoku-Oki earthquake are identical to those before it. Beyond
174 this constant parameter correction, a correction is also performed with the new model
175 parameters obtained from the period following the Tohoku-Oki earthquake, which covers the
176 period of the anomaly. The assumption behind this second correction is that the sensitivities
177 to the hydro-meteorological factors change due to the crustal deformation induced by the
178 earthquake. Thus, the contributions of the hydro-meteorological forcings to the seismic
179 velocities might be different from those before the earthquake. The postseismic
180 environmental-effect correction is applied after the time series is detrended to remove the
181 effects of the coseismic and postseismic long-term tendencies. The parameters for this
182 correction are determined to minimize the velocity fluctuations, and are based on the actual
183 time series of local observations for precipitation, snow, and sea-surface height. The time

184 interval used covers the period of the anomaly. Hence, this correction optimizes the removal
185 of the anomaly.

186

187 We show in Appendix (Figure A1) the corrected seismic velocity changes from each station
188 by gray curves. In global, this anomaly is evident from abundant stations, especially stations
189 with high coseismic velocity drops. Figure 1b shows the averaged time series of seismic
190 velocity changes over the 236 Hi-net stations without and with the external effect corrections.
191 It can be seen from that without or with the model corrections, the influence on the averaged
192 anomalous velocity decreases is subtle. The secondary velocity drop persists after both of
193 these environmental effect corrections. The amplitudes of the anomaly after the corrections
194 are still comparable to the changes due to the inland Iwate-Miyagi Nairiku earthquake in
195 2008. The preserved anomaly confirms the interpretation of the second drop as the evidence
196 of changes in the physical properties of the medium that are not governed by environmental
197 factors. In the following, we consider the seismic velocity time series that is corrected with
198 the model which is parameterized based on the years preceding the anomaly (Wang et al.,
199 2017) as corrected velocity changes, and with the local meteorological and oceanographic
200 observations as input.

201

202 Figure 1c, d show the maps of the differences of the averaged seismic velocities during the
203 two episodes indicated in Figure 1b (green and orange shading), without any corrections
204 (Figure 1c) and after the correction with the constant parameters (Figure 1d). From these
205 maps of the spatial distributions of the velocity differences, it can be seen that before the
206 correction, the anomaly was mainly along the central volcanic axis (Figure 1c). When the
207 correction based on the data before the Tohoku-Oki earthquake is applied, the anomaly is still
208 extensive across the set of stations, and the overall feature is preserved (Figure 1d). The

209 distribution characteristics confirm that this velocity reduction occurs in the volcanic area and
210 its vicinity. The particularity of the geographical location of the volcanos and the surrounding
211 area is an essential feature of this velocity anomaly. After discarding the external forcings as
212 the possible source of these observations, the deep origins of this secondary velocity drop
213 anomaly of ~0.01% are investigated. To clarify this question, we discuss the possible causes
214 of the second drop in the light of different independent observations from occurrence of
215 regular seismicity and LFEs in the Honshu island, and from tilt recordings and fault strength
216 in small scale.

217

218 **3. Nonlinear responses to earthquake ground motion**

219

220 Strong ground motions induced by earthquake shaking affect shallow seismic velocities
221 (Poupinet et al., 1984; Schaff & Beroza, 2004; Peng & Ben-Zion, 2006; Sens-Schönfelder &
222 Wegler, 2011; Brenguier et al., 2014; Sawazaki et al., 2015; Wang et al., 2019). We take
223 advantage of the JMA catalog within latitudes 34°N – 42°N and longitudes 138°E – 143°E, to
224 convert the seismic magnitudes into the corresponding seismic intensities of shaking and to
225 compare their relationship with the seismic velocity changes. As Katsumata (1996) and
226 Uchide & Imanishi (2018) have reported, there are some systematic differences in the
227 magnitude scales between the M_{JMA} and the conventional moment magnitude M_w . Therefore,
228 we first transformed the M_{JMA} into M_w for $0.5 \leq M_{JMA} \leq 7.0$ using Equation (1), as proposed
229 by Uchide & Imanishi (2018):

230

$$231 \quad M_w = aM_{JMA}^2 + bM_{JMA} + c \quad (1),$$

232

233 where parameters a, b, and c are 0.053, 0.33, and 1.68, respectively. We then evaluated the
234 moment according to Equation (2), from Hanks & Kanamori (1979):

235

$$236 \quad M_0 = 10^{(M_w * 1.5 + 9.05)} \quad (2).$$

237

238 Then we compare the corrected velocity time series with the ground motion deduced from the
239 moments. For each seismic moment observation, the intensity of the shaking is evaluated
240 from the approximate ground velocity. We assume the classical scaling of M_0 with the cube
241 of the duration and the constant stress drop. Therefore, we propose Equation (3) to calculate
242 the normalized cumulative intensity (I), considering both the geometric decay and the
243 nonelastic attenuation from the hypocenters to the seismic stations.

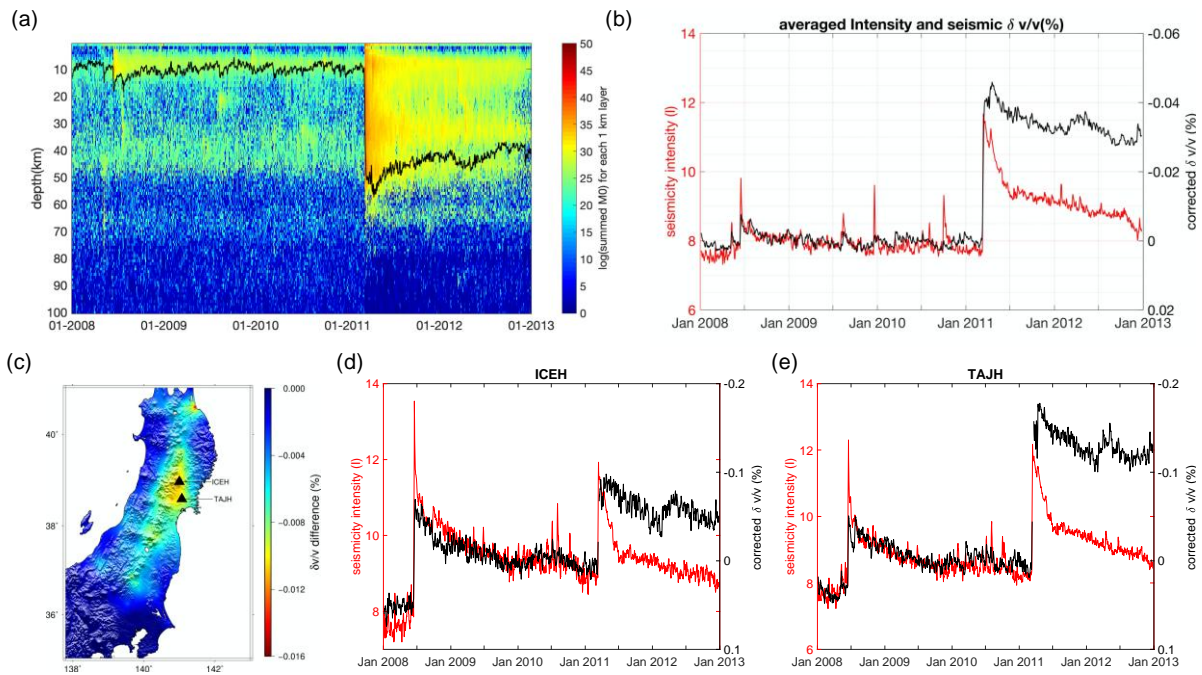
244

$$245 \quad (I)_i = \left\{ \sum_{n=1}^{N_i} \left(M_{0n}^{1/3} * \frac{1}{r_n^j} \right) \right\} e^{-t_n/t^*} \quad (3),$$

246

247 where M_{0n} is the seismic moment, r_n is the distance to the hypocenter, t_n is the travel-time
248 from source to station with a velocity of 3 km/s for every event n, t^* is to account for the
249 nonelastic attenuation, i is the i^{th} day in the time series, N_i is the total number of events for
250 day I, and j is the exponent of distance in the geometric spreading factor. In this study, we set
251 j as 1.0, on the assumption of body waves and t^* as 50 s for an empirical value. Note that in a
252 far-field approximation for shear waves, the ground velocity is proportional to the dynamic
253 stress.

254



255

256 **Figure 2.** (a) Comparison of M_0 within latitudes $34^\circ\text{N} - 42^\circ\text{N}$ and longitudes $138^\circ\text{E} - 143^\circ\text{E}$ and the seismic
 257 velocity changes. M_0 is normally summed within each 1-km layer, and changes with time at different depths,
 258 down to 100 km. For these data, the two-dimensional adaptive noise-removal Wiener filter (Matlab built-in
 259 Wiener2) was applied, with the parameter as 5 in both dimensions. Black curve, normally averaged corrected
 260 seismic velocity changes over all of the 236 Hi-net stations. (b) Comparison of the daily time series of the
 261 averaged-corrected seismic velocities with the daily time series of the averaged seismic intensity calculated with
 262 the seismic events without depth restrictions and t^* of 50 s. (c) Map of the secondary drop anomaly and
 263 locations of stations ICEH and TAJH. (d, e) Comparisons between the time series of the seismic intensity (I)
 264 and the seismic velocity changes at stations ICEH (d) and TAJH (e). To both of these time series we applied a
 265 moving-average filter with a window size of 4 days.

266

267 Here, we first calculate the summed seismic moments within each kilometer of depth for each
 268 day. Figure 2a shows that the seismic events mainly occur within the first 50 km in depth,
 269 and before the Tohoku-Oki earthquake, they show two concentrations of activity at depths of
 270 around 10 km and 40 km. Within the first 2 years from the mainshock, this deepens to 70 km,
 271 with a different depth distribution. To visually understand the relationship between the
 272 changes in the seismic velocity and the changes in the seismic intensity, I , with time and

273 depth, the spatially averaged-corrected seismic velocity changes are plotted on the image of
274 the seismic moment in Figure 2a. Positive global correlation between these two observations
275 is seen before the mainshock. One month after the main shock, there is also a strong
276 correlation between intensity from large aftershocks and seismic velocity, leading to the
277 lowest seismic velocity reached. Nevertheless, when the early 2012 anomaly appears, there is
278 no apparent enhanced seismicity.

279

280 Figure 2b compares the averaged seismic velocity changes for the whole network with the
281 averaged intensities of the ground motion calculated from every station in Figure 2a. The
282 velocity time series are corrected for environmental effects. For visual convenience, the
283 direction of the velocity changes has been reversed here. There is correlation between the
284 changes in the seismic velocity and the seismic intensity, which is particularly striking before
285 and just after the Tohoku-Oki earthquake. Dynamic stress from earthquakes shaking appears
286 to be the main control of rapid velocity during this period.

287

288 After the main shock, there is a decrease in the daily ground motion intensity that is related to
289 the aftershock decay. There is also a corresponding general increasing trend in the velocity,
290 although the correlation between the velocity and the earthquake motion intensity is weak,
291 and there is no evidence of a correlation with the early 2012 delayed drop in the velocity; this
292 suggests that the anomalous velocity drop is not related to the seismic ground motion. Here,
293 we just use the averaged velocity and the ground motion evaluated at a single point, while
294 local events might strongly control the ground motion for each station. We also present the
295 same comparison for specific sites of stations ICEH and TAJH, where the delayed velocity
296 drops have large amplitudes. The ground motion intensity is computed specifically for each
297 of these locations. Figure 2d and e show the comparisons of the velocity changes and the

298 seismic intensities at the ICEH and TAJH stations after smoothing with a 4-day moving time
299 window. Correlations of the velocity drops with the earthquake activity can be seen before
300 the main event. Even the fluctuations with characteristic times of several months correlate
301 well with the seismic motion. However, for the anomalous velocity drops in 2012, there is no
302 correspondence between the time evolution of the intensity of ground motion and that of the
303 velocity. Notably, in Figure 2d, there is also a correlation between the seismic velocity
304 decrease and the slightly increased seismic intensity envelop in around July 2010, which is
305 mainly controlled by the local earthquake events near station ICEH. We can see that this
306 correlation has tightened and disappeared at the end of 2010. Nevertheless, this local feature
307 is not dominant in the averaged comparison in Figure 2b. For these different single stations
308 and the averaged data, it appears that there are other processes at work in addition to the
309 velocity relaxation and seismicity, which have to be invoked to explain the secondary drop
310 that occurs in early 2012.

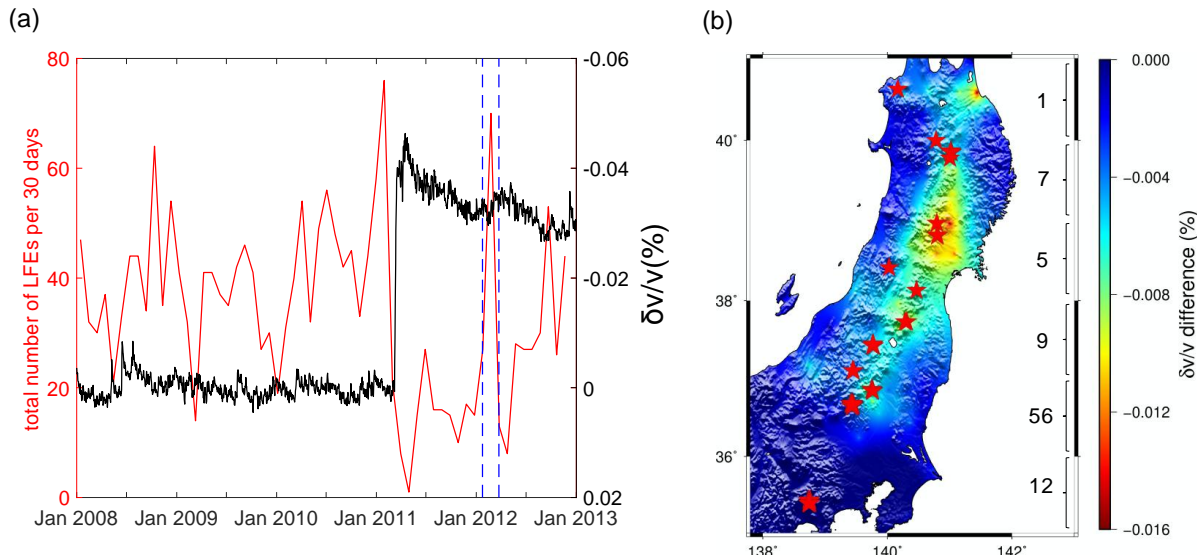
311

312 **4. Comparisons with low-frequency earthquakes**

313

314 As the process responsible for the secondary velocity drop is located along the volcanic chain,
315 we check the small seismic activity associated with volcanic activity, in the form of (LFEs).
316 The origins of volcanic LFEs are interpreted in relation to the magma activities (Aki et al.,
317 1977; Chouet et al., 1987; Hasegawa & Yamamoto, 1994; Nakamichi et al., 2003, 2004) or to
318 both migration of crustal fluids and local magma that ascends in southwest Japan beneath the
319 active arc volcanoes (Yu et al., 2018). Furthermore, Aso et al. (2013) report that LFEs
320 beneath Osaka Bay which is out of the volcanic areas are due to fluid upwelling from the
321 mantle. For more general perspectives, LFEs are related to the pressure changes generated by
322 fluid-flow transients (Katsumata & Kamaya, 2003; Shapiro et al., 2018). We use the JMA

323 catalog of manually detected LFEs. The depth distribution of these LFEs is from 10 km to 40
 324 km. We sum the daily number of LFEs for a 30-day window within the study area. The
 325 monthly activities of the LFEs are presented in Figure 3a.



326
 327 Figure 3. (a) Total number of low-frequency earthquakes (LFEs) over each 30-day window, and the averaged
 328 seismic velocity changes over the 236 stations in Honshu. (b) Map of the secondary velocity drop and the
 329 locations of the epicenters of all the LFEs in the time period between the two vertical blue dashed lines in (a)
 330 (January 24, 2012 to March 24, 2012; determined by the times of the peaks). The numbers on the right are
 331 summed numbers of LFEs per degree of latitude.

332
 333 From Figure 3a, the overall number of LFEs appears to drop after the Tohoku-Oki earthquake
 334 (Tokuda & Shimada, 2019), which possibly indicates a change in the physical state of the
 335 crust. This might be related to the significant extension of continental crust by the anelastic
 336 deformation produced by the event (Tsuji et al., 2013). On the other hand, it needs to be
 337 carefully considered whether the intense aftershock activity might affect the detection level.
 338 Figure 3a (black) also shows the seismic velocity changes averaged over all of the 236 Hi-net
 339 stations. During the period when the seismic wave velocity starts to decrease in early 2012,
 340 the number of LFEs rapidly increases. The decrease in the velocity and the enhanced LFEs

341 activity are simultaneous. These observations support the hypothesis that our observations of
342 the seismic velocity are related to fluid transfer in the upper part of the crust.

343

344 Figure 3b shows the epicenters of all of the LFEs in Figure 3a from January 24, 2012 to
345 March 24, 2012 (indicated by the two blue dashed lines). This is the period covering both the
346 sudden increase in LFEs and the decay of the seismic velocity. A large number of the LFEs
347 during this period occur at very close locations and the epicenters are superimposed on the
348 map. We show the counted numbers of LFEs per latitude on the side of Figure 3b. A big part
349 of LFEs locates in the area within 36°N and 37°N , and others are mainly along the central
350 volcanic chain, which coincides with the area where the major seismic velocity decrease
351 anomaly occurred in early 2012. Despite the concentration of LFEs in the southern part of the
352 velocity anomaly, these two global spatial distributions are not limited to a small area but
353 cover the wide region of the volcanic chain of Honshu Island. The agreement in both space
354 and time provides further support for our interpretation that this decrease in seismic wave
355 velocity is closely related to deep fluid movement. However, as of the manually-picked
356 catalog of LFEs, the actual number could be underestimated. It should be noted that the depth
357 distribution of LFEs is likely deeper than the layer probed by the waves used in our velocity
358 measurements and is not directly linked to the depth of changes in velocity. Nevertheless, we
359 suggest that further careful cross-investigation on the correlation of LFEs and changes in
360 seismic velocity is important to disclose the stress state of the crust.

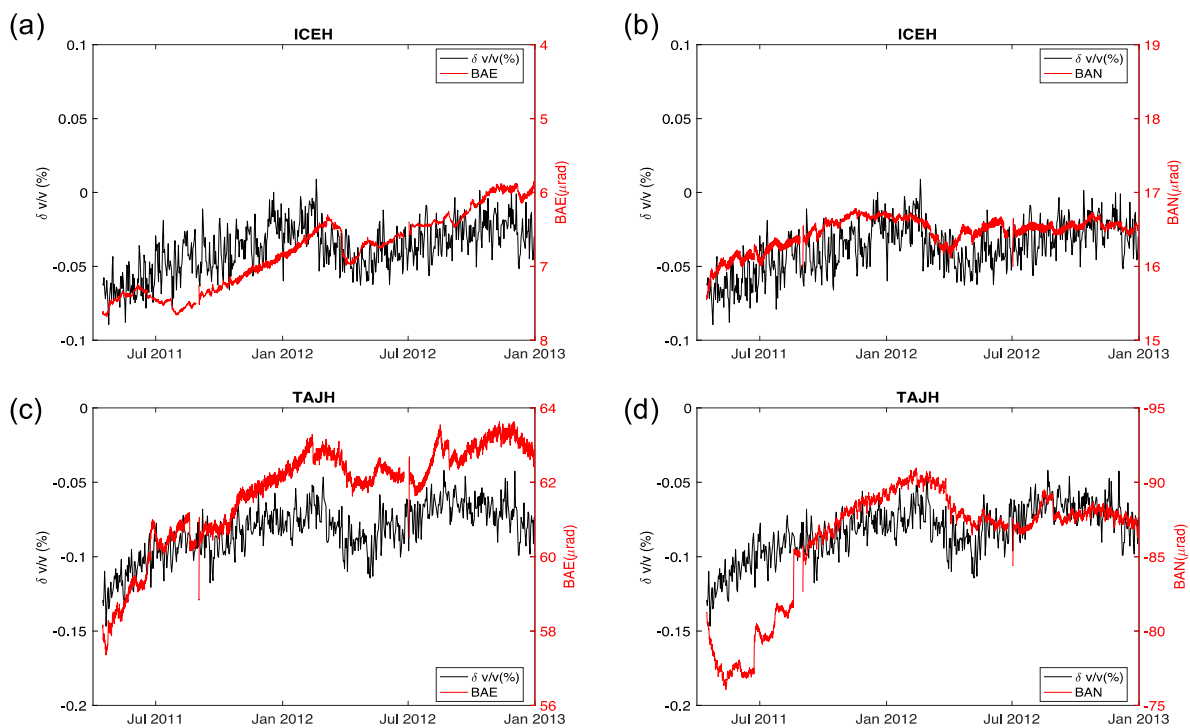
361

362 **5. Tiltmeter recordings**

363

364 The Hi-net tiltmeters located in the same boreholes as those for the short period seismic data
365 are used to directly compare the relationship between the seismic velocity changes and the

366 ground tilt. Tiltmeters are sensitive to variations of fluid contents or fluid pressures due to
 367 different processes, such as groundwater level changes due to precipitation (Sato et al., 1980)
 368 and volcanic fluid motion (Ueda et al., 2005). Tiltmeter recordings should give more precise
 369 information on local subtle deformation than GPS displacement (e.g., Dzurisin, 2003). We
 370 took advantage of these co-sited tiltmeters to see how the ground tilt varies during the
 371 velocity anomaly period.
 372



373
 374 **Figure 4.** Comparisons between the seismic velocity changes and the ground tilt at Hi-net stations ICEH (a, b)
 375 and TAJH (c, d) for the two horizontal components. Both time series are positively correlated, except for (a) and
 376 (d), where the tilt is plotted upside-down to illustrate the similar anomaly. BAN and BAE are the two horizontal
 377 components in directions of N-S and E-W, respectively.

378
 379 The raw daily data is first down sampled to 0.02 Hz and a low-pass with a frequency 0.4-fold
 380 the decimation frequency. Then, we compare the 2-year data with the velocity measurements
 381 at the ICEH and TAJH stations, for which the correlations between the velocity changes and

382 the seismic intensities have already been discussed and that exhibit large amplitudes for the
383 secondary velocity drop (see Figure 2b). In the shallow part of the crust, the deep fluid
384 upwelling is likely to be localized in the volcano feeding zones. Under these conditions, the
385 relative positions of the tiltmeters with respect to fluid upwelling determine the polarity of
386 the recordings. This is the reason why the results are present with arbitrary polarities, to
387 highlight the identifiable corresponding observations between the seismic velocities and the
388 ground tilt.

389

390 After gap filling, the tiltmeter raw data are low-pass filtered to focus on the daily changes in
391 the ground tilt. The comparisons between velocity and tilt changes are shown in Figure 4.
392 Except for Figures 4a and d, the tilt recordings are plotted upside-down. The data in the other
393 Figures are represented conventionally. The time series of the changes in the seismic
394 velocities and ground tilt show striking common features. Both the long-term trends and the
395 short-term transient changes are almost identical to each other over the 2-year postseismic
396 period. The tilt recordings from the E-W components change by $\sim 1 \mu\text{rad}$ at both stations, and
397 during the second drop period, the N-S component changes by $\sim -3 \mu\text{rad}$ at TAJH and ~ 0.5
398 μrad at ICEH.

399

400 These simultaneous changes in the seismic velocity and the ground tilt indicate that the
401 ground tilt is useful to confirm subtle local changes in seismic velocities. However, due to the
402 instability of the tiltmeter data at the different locations, and due to the very local nature of
403 the measures, a few sites show such similar functional correlations, but not all of them. There
404 are no systematic changes with the same anomaly for all stations. Nevertheless, it is worth
405 emphasizing that this is the first observation of a strong correlation between seismic velocity
406 changes and ground tilt. We also check the GPS time series of the displacements. No

407 equivalent changes to the tilt highlight this velocity change anomaly. Our conclusion is
408 consistent with the discussion by Lesparre et al. (2017) that tiltmeter has higher resolutions
409 on detecting the small-scale deformation and internal motion than the geodetic methods such
410 as GPS, which works when the strain is sufficiently big in large scale.

411

412 Based on the parallel evolution in seismic velocity and tilt, we can conclude that both the
413 local tilt and the velocity changes share the same physical origin. This deformation might be
414 in the volcanic system, as station ICEH is close to the central volcanic chains. The
415 deformation might also be due to fluid transport in the crust, as observed with the migration
416 of seismicity studied by Yoshida et al. (2019), or with the fluid upwelling through fractured
417 rock zones (Aso et al., 2013).

418

419 **6. Further seismological evidence**

420

421 We show that the cause of the anomalous velocity drop is also distinguishable in local ground
422 tilt records for some stations. At the same time, there is also a significant increase in LFEs in
423 the volcanic area in Honshu. The spread distribution of both the LFEs and the velocity
424 anomaly in Honshu might relate to fluid migration after the Tohoku-Oki earthquake. In this
425 section, we recall the depth-dependent seismic velocity changes by Wang et al. in 2019 and
426 discuss some further seismological evidence of changes in the fault strength from an
427 earthquake swarm in Honshu and the fluid-driven swarms that widely exist in Honshu.

428

429 Yoshida et al. (2016, 2017, 2019) report on temporal variations of fault strength calculated
430 using an earthquake swarm in central Honshu. The change in fault strength results from fluid
431 migration starting after the Tohoku-Oki earthquake. Hypocenters in the earthquake sequence

432 exhibit a distinct migration behavior analogous to the fluid-injection induced seismicity,
433 which supports this hypothesis. All of these studies prove that in the volcanic area, large
434 earthquakes trigger many seismic clusters and pore pressure changes with time, due to the
435 fluid migration. These changes have continuity and directivity of both their temporal and
436 spatial distributions.

437

438 We refer now to the time series of fault strength data in Figure 13 of Yoshida et al. (2016).
439 There is an immediate drop in the fault strength following the mainshock. As time goes by
440 after the Tohoku-Oki earthquake, the strength tends to recover gradually, while there is an
441 anomalous drop of ~10% that started from around 350 days after the earthquake in early 2012.
442 This drop of fault strength is synchronous to the simultaneous seismic velocity anomaly. We
443 discuss in detail in the Appendix the relationship between the fault strength and the seismic
444 velocity changes in the same region, the southern limitation of velocity anomaly, where there
445 is also the concentration of LFEs. Due to the sensitivity of tilt to changes in fluid and the
446 simultaneous drop in fault strength, we infer that the main cause of this second drop anomaly
447 is an increase in pore pressure.

448

449 As well as their observations of the local earthquake swarms, Okada et al. (2015) studied
450 some widely distributed regional earthquakes along the volcanic axis in Honshu after the
451 Tohoku-Oki earthquake. They concluded that there is migration of the hypocenters of
452 earthquake swarms driven by changes in crustal fluid distribution and permeability. Kosuga
453 (2014) report on the spatiotemporal migration of seismic activity near the Moriyoshi-zan
454 volcano in north-eastern Japan, with the implication of geofluid migration and a mid-crustal
455 fluid reservoir. When the Tohoku-oki earthquake occurred, there was rapid regional

456 extension of the crust. Such extension of the crust and changes in crustal permeability led to a
457 loss of equilibrium of the fluid system.

458 In a previous paper (Wang et al., 2019), we have investigated depth-dependent time series of
459 seismic velocity changes after the Tohoku-oki earthquake (Figure 8 of Wang et al., 2019),
460 We found indications of a delayed velocity drop propagating from the deep part up to the
461 shallow part and we have suggested a possible upward fluid flow, which may control the
462 decreases in seismic velocity. Based on the inverted velocity changes at depth, we speculate
463 that the arrival of upward fluid in the shallow crust from the mantle is responsible for the
464 secondary velocity decreases in early 2012 widely spread over the volcanic chain. Assuming
465 a diffusion process, to relate the distance from the source of the fluids and the time required
466 for the diffusion front to propagate, we rely on Equation (4) (e.g., Shapiro et al., 1997):

467

$$468 \quad r = \sqrt{4\pi Dt} \quad (4),$$

469

470 where r is the distance from the source of the fluids, t is the time required for the diffusion
471 front to propagate, and D is the diffusivity of the pore pressure. Considering a distance of 20
472 km from the lower crust, where the depth represents a reservoir of high-pressure for fluids
473 released up to the surface, the duration of fluid propagation is around 11 months, the
474 corresponding average diffusivity is of the order of $1 \text{ m}^2/\text{s}$. This value is in the range of the
475 calculated diffusivity $0.4 - 1.5 \text{ m}^2/\text{s}$ by Kitagawa et al. (2007) near the Nojima fault zone in
476 Japan after the M_w 7.2, 1995 Kobe earthquake.

477

478 Based on the consistency between the reduction in the fault strength and the velocity decrease,
479 we can conclude that increase in pore pressure produced by up-moving fluid is responsible
480 for the drops in velocity in 2012. Thus, there appears to be an increase in seismic events

481 during this period. However, this lacks direct correlation between dynamic stress from
482 earthquakes and the velocity changes. The decrease in the velocity and the temporary
483 increase in the seismic events are both the results of changes in pore pressure due to fluid
484 motion.

485

486 **7. Discussion and conclusion**

487

488 Here, we have focused on the anomaly of very localized seismic wave velocity changes near
489 the central volcanic chain of Honshu Island in Japan. This anomaly occurs about 11 months
490 after the 2011 Tohoku-Oki Earthquake. We observe a seismic velocity anomaly that is
491 comparable to that associated with the inland M_w 6.8 Iwate-Miyagi Nairiku shallow
492 earthquake in 2008. However, there is a lack of direct explanation as coseismic change from
493 any significant earthquake occurrence. Moreover, this velocity decrease is not instantaneous,
494 but shows a continuous slowdown over several months.

495

496 To explain this anomaly, we analyze the changes in the surrounding environmental and use
497 two linear models to correct possible changes in seismic velocity based on the local
498 meteorological and oceanographic recordings. The remained velocity decrease helps
499 excluding the anomaly from being an effect of environment-induced changes. Further study
500 on the earthquake moment intensity takes into account the geometric and inherent attenuation.
501 We find that the changes in the moment intensity and seismic wave velocity before the
502 Tohoku-Oki earthquake show an excellent linear correlation. However, there is an absence of
503 vigorous moment intensity during the anomaly to directly explain the velocity decrease
504 anomaly. By comparison with LFE activity, the consistency of the temporal and spatial
505 distributions suggests shared physical origins of concentration of the LFEs and the velocity

506 drop. Further observations of the ground tilt from the co-sited Hi-net tiltmeters confirm the
507 independently measurable physical changes in the crust that are responsible for the velocity
508 anomaly. As the ground tilt is under the influence of local changes, through this comparison
509 and the above analysis, we believe that the localized velocity decrease observed is related to
510 fluid activities in the volcanoes, or their fault systems, where the presence of a crack makes
511 the flow of deep fluids easier. Additionally, we show a small scale decrease in fault strength
512 driven by the earthquake swarms related to the fluid activities. By considering a simple fluid
513 diffusion process, we obtain a diffusion coefficient in the order of $1 \text{ m}^2/\text{s}$. This assumes fluid
514 migrating through the crust following the crustal extension induced by the Tohoku-Oki
515 earthquake. The fluid migration generates not only increases in fluid-driven swarm seismicity
516 and LFEs in Honshu, but also pore pressure, and hence decreases in seismic wave velocities
517 in the same regions.

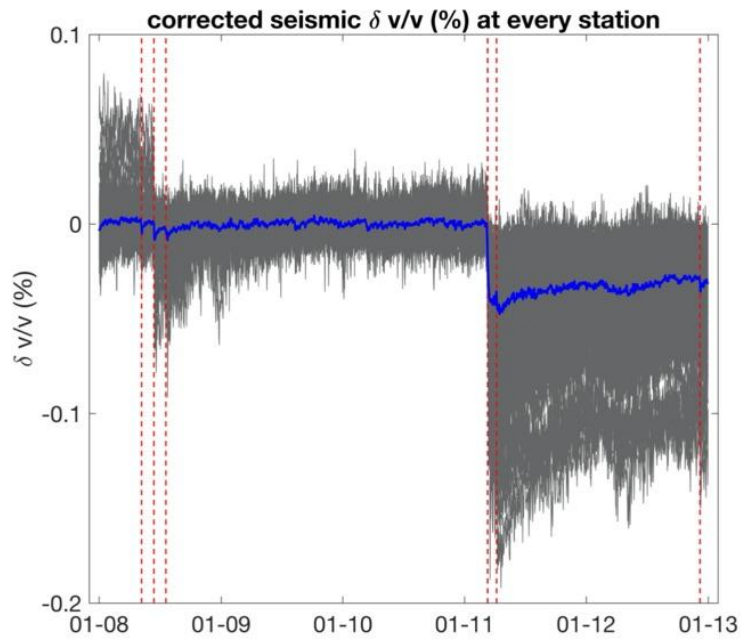
518 **Acknowledgements**

519 The authors want to thank Mariano Supino for the contribution on LFEs catalog, Hisashi
520 Nakahara, Takeshi Nishimura, Kiwamu Nishida, Yosuke Aoki, and Kaoru Sawazaki for
521 fruitful discussions. Q.-Y. Wang specially thanks William Frank for the support on finishing
522 this paper. This work was supported by the European Research Council (ERC) under the
523 European Union Horizon 2020 Research and Innovation Program (Grant Agreement 742335,
524 F-IMAGE). Most of the computations presented in this paper were performed using the
525 GRICAD infrastructure (<https://gricad.univ-grenoble-alpes.fr>), which is supported by
526 Grenoble research communities.

527

528 **Data availability**

529 The Hi-net seismic and tilt data used here are available from the National Research Institute
530 for Earth Science and Disaster Prevention (NIED, <http://www.hinet.bosai.go.jp>).

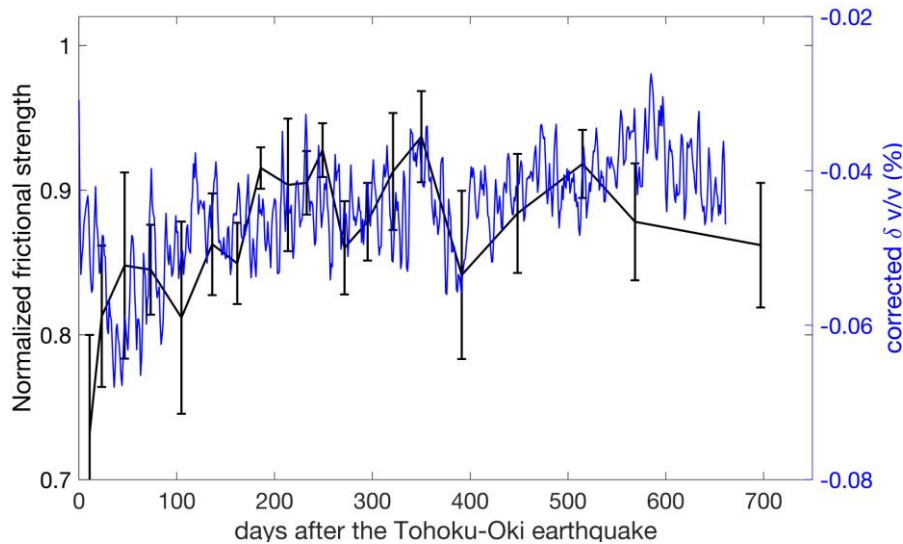


532

533 **Figure A1.** Corrected seismic velocity changes from 236 Hi-net stations in Figure 1a. The blue curve is the
534 averaged time series over the 236 stations. The red vertical dashed lines indicate the six earthquakes indicated in
535 Figure 1a.

536

537



538

539 **Figure A2.** Comparison of the fault strength (error bars calculated by Yoshida et al. (2016) using earthquake
 540 swarms around Hi-net station ATKH) at a volcanic site and the seismic velocity changes at station ATKH.
 541 Black curve, calculated fault strength with error bars; blue curve, 5-day moving average smoothed seismic
 542 velocity changes after removing environmental effects; red shaded area, anomalous period ~350 days after the
 543 Tohoku-Oki earthquake in early 2012.

544

545 We refer to the changes in fault strength calculated by Yoshida et al. (2016) in a volcanic
 546 area using the earthquake swarms from the day of the Tohoku-Oki earthquake until 700 days
 547 after the earthquake. As the time increases, there are fewer seismic events. Hence, the
 548 interval of the binned plot gets larger, and the accuracy can also decrease. Nevertheless, there
 549 is a clear drop in the fault strength from day ~350 after the mainshock (Figure A2). This
 550 decrease happens at the same time as the secondary velocity drop distributed in the volcanic
 551 areas.

552

553 Then we compare the strength time series with the seismic velocity changes after correcting
 554 for the possible environmental perturbation-related changes at the ATKH Hi-net station. This
 555 station is located in the center of the earthquake swarm. Figure A2 shows the fault strength
 556 and the residuals of the seismic velocity changes after the changes related to external forcing

557 have been removed. There is an apparent decrease of $\sim 0.015\%$ in the seismic velocity for the
558 days around 300 to 400. In this same time period, there is an $\sim 10\%$ decrease in the
559 normalized fault strength. This simultaneous change indicates that the velocity drop and the
560 strength drop are due to the same physical process. This process involves an increase in the
561 pore pressure associated with the upwelling flow of deep fluid that was triggered by the
562 Tohoku-oki earthquake and reached the shallow crust about 11 months later.

563 **References**

564

565 Aki, K., Fehler, M., Das, S. 1977. Source mechanism of volcanic tremor: fluid-driven crack
566 models and their application to the 1963 Kilauea eruption. *Journal of Volcanology and*
567 *Geothermal Research.* 2, 259-287. [https://doi.org/10.1016/0377-0273\(77\)90003-8](https://doi.org/10.1016/0377-0273(77)90003-8)

568 Aso, N., Ohta, K., Ide, S. 2013. Tectonic, volcanic, and semi-volcanic deep low-frequency
569 earthquakes in western Japan. *Tectonophysics.* 600, 27-40.
570 <https://doi.org/10.1016/j.tecto.2012.12.015>

571 Brenguier, F., Campillo, M., Hadziioannou, C., Shapiro, N.M., Nadeau, R.M., Larose, E.
572 2008. Postseismic relaxation along the San Andreas fault at Parkfield from continuous
573 seismological observations. *Science.* 321(5895), 1478-1481.
574 <https://doi.org/10.1126/science.1160943>

575 Brenguier, F., Campillo, M., Takeda, T., Aoki, Y., Shapiro, N.M., Briand, X., et al. 2014.
576 Mapping pressurized volcanic fluids from induced crustal seismic velocity drops.
577 *Science.* 345(6192), 80-82. <https://doi.org/10.1126/science.1254073>

578 Chen, J.H., Froment, B., Liu, Q.Y., Campillo, M. 2010. Distribution of seismic wave speed
579 changes associated with the 12 May 2008 M_w 7.9 Wenchuan earthquake. *Geophys. Res.*
580 *Lett.*, 37, L18302, <https://doi.org/10.1029/2010GL044582>

581 Chouet, B., Koyanagi, R.Y., Aki, K. 1987. Origin of volcanic tremor in Hawaii. Part II.
582 Theory and discussion. US Geological Survey Professional Paper. Chapter 45, 1259-
583 1279.

584 Donaldson, C., Winder, T., Caudron, C., White, R.S. 2019. Crustal seismic velocity responds
585 to a magmatic intrusion and seasonal loading in Iceland's Northern Volcanic Zone.
586 *Science Advances*, 5(11). <https://doi.org/10.1126/sciadv.aax6642>

587

588 Dzurisin, D. 2003. A comprehensive approach to monitoring volcano deformation as a
589 window on the eruption cycle. *Reviews of Geophysics*. 41, 1001.
590 <https://doi.org/10.1029/2001RG000107>

591 Froment, B., Campillo, M., Chen, J.H., Liu, Q.Y. 2013. Deformation at depth associated with
592 the 12 May 2008 M_w 7.9 Wenchuan earthquake from seismic ambient noise monitoring.
593 *Geophys. Res. Lett.* 40, 78-82. <https://doi.org/10.1029/2012GL053995>

594 Hanks, T.C., Kanamori, H. 1979. A moment magnitude scale. *J. Geophys. Res.*, 84(B5),
595 2348-2350, <https://doi.org/10.1029/JB084iB05p02348>.

596 Hasegawa, A., Yamamoto, A. 1994. Deep, low-frequency microearthquakes in or around
597 seismic low-velocity zones beneath active volcanoes in northeastern Japan.
598 *Tectonophysics*. 233(3-4), 233-252. [https://doi.org/10.1016/0040-1951\(94\)90243-7](https://doi.org/10.1016/0040-1951(94)90243-7)

599 Hillers, G., Campillo, M., Ma, K.F. 2014. Seismic velocity variations at TCDP are controlled
600 by MJO driven precipitation pattern and high fluid discharge properties. *Earth Planet. Sci.*
601 *Lett.* 391, 121-127. <https://doi.org/10.1016/j.epsl.2014.01.040>

602 Hillers, G., Ben-Zion, Y., Campillo, M., Zigone, D. 2015. Seasonal variations of seismic
603 velocities in the San Jacinto fault area observed with ambient seismic noise. *Geophys. J.*
604 *Int.* 202(2), 920-932. <https://doi.org/10.1093/gji/ggv151>

605 Hobiger, M., Wegler, U., Shiomi, K., Nakahara, H. 2012. Coseismic and postseismic elastic
606 wave velocity variations caused by the 2008 Iwate-Miyagi Nairiku earthquake, Japan. *J.*
607 *Geophys. Res.* 117, B09313. <https://doi.org/10.1029/2012JB009402>

608 Katsumata, A. 1996. Comparison of magnitudes estimated by the Japan meteorological
609 agency with moment magnitudes for intermediate and deep earthquakes. *Bulletin of the*
610 *Seismological Society of America*. 86 (3): 832-842.

611 Katsumata, A., Kamaya, N. 2003. Low-frequency continuous tremor around the Moho
612 discontinuity away from volcanoes in the southwest Japan. *Geophys. Res. Lett.* 30(1),
613 1020. <https://doi.org/10.1029/2002gl015981>

614 Kitagawa, Y., Fujimori, K., & Koizumi, N. 2007. Temporal change in permeability of the
615 Nojima fault zone by repeated water injection experiments. *Tectonophysics.* 443, 183-
616 192. <https://doi.org/10.1016/j.tecto.2007.01.012>

617 Kosuga, M. 2014. Seismic activity near the Moriyoshi-zan volcano in Akita Prefecture,
618 northeastern Japan: implications for geofluid migration and a midcrustal geofluid
619 reservoir Geofluid processes in subduction zones and mantle dynamics. *Earth Planet Sp.*
620 66, 77. <https://doi.org/10.1186/1880-5981-66-77>

621 Lesparre, N., Boudin, F., Champollion, C., Chéry, J., Danquigny, C., Seat, H. C., et al. (2017).
622 New insights on fractures deformation from tiltmeter data measured inside the Fontaine
623 de Vaucluse karst system. *Geophys. J. Int.* 208(3), 1389-1402,
624 <https://doi.org/10.1093/gji/ggw446>

625 Meier, U., Shapiro, N.M., Brenguier, F. 2010. Detecting seasonal variations in seismic
626 velocities within Los Angeles basin from correlations of ambient seismic noise. *Geophys.*
627 *J. Int.* 181(2), 985-996. <https://doi.org/10.1111/j.1365-246X.2010.04550.x>

628 Nakamichi, H., Hamaguchi, H., Tanaka, S., Ueki, S., Nishimura, T., Hasegawa, A. 2003.
629 Source mechanisms of deep and intermediate-depth low-frequency earthquakes beneath
630 Iwate volcano, northeastern Japan. *Geophys. J. Int.* 154 (3), 811-828.
631 <https://doi.org/10.1046/j.1365-246X.2003.01991.x>

632 Nakamichi, H., Ukawa, M., Sakai, S. 2004. Precise hypocenter locations of midcrustal low-
633 frequency earthquakes beneath Mt. Fuji, Japan. *Earth Planet Sp.* 56, e37-e40.
634 <https://doi.org/10.1186/bf03352542>

635 Obara, K., Kasahara, K., Hori, S., Okada, Y. 2005. A densely distributed high-sensitivity
636 seismograph network in Japan: Hi-net by National Research Institute for Earth Science
637 and Disaster Prevention. *Review of Scientific Instruments*. 76.
638 <https://doi.org/10.1063/1.1854197>

639 Obermann, A., Froment, B., Campillo, M., Larose, E., Planès, T., Valette, B., et al. 2014.
640 Seismic noise correlations to image structural and mechanical changes associated with
641 the M_w 7.9 2008 Wenchuan earthquake. *J. Geophys. Res.: Solid Earth*, 119(4), 3155-
642 3168. <https://doi.org/10.1002/2013JB010932>

643 Okada, T., Matsuzawa, T., Umino, N., Yoshida, K., Hasegawa, A., Takahashi, H., et al. 2015.
644 Hypocenter migration and crustal seismic velocity distribution observed for the inland
645 earthquake swarms induced by the 2011 Tohoku-Oki earthquake in NE Japan:
646 implications for crustal fluid distribution and crustal permeability. *Geofluids*. 15, 293-
647 309. <https://doi.org/10.1111/gfl.12112>

648 Okada, Y., Kasahara, K., Hori, S., Obara, K., Sekiguchi, S., Fujiwara, H., Yamamoto, A.
649 2004. Recent progress of seismic observation networks in Japan - Hi-net, F-net, K-net
650 and KiK-net. *Earth Planet Sp.* 56, xv-xxviii. <https://doi.org/10.1186/BF03353076>

651 Peng, Z., Ben-Zion, Y. 2006. Temporal changes of shallow seismic velocity around the
652 Karadere-Düzce branch of the north Anatolian fault and strong ground motion. *Pure appl.*
653 *geophys.* 163, 567-600. <https://doi.org/10.1007/s00024-005-0034-6>

654 Poli, P., Marguin, V., Wang, Q.-Y., D'Agostino, N., Johnson, P. 2020. Seasonal and
655 coseismic velocity variation in the Region of L'Aquila from single station measurements
656 and implications for crustal rheology. *Journal of Geophysical Research: Solid Earth*.
657 125(7). <https://doi.org/10.1029/2019jb019316>

658 Poupinet, G., Ellsworth, W.L., Frechet, J. 1984. Monitoring velocity variations in the crust
659 using earthquake doublets: an application to the Calaveras Fault, California. *J. Geophys.*
660 *Res.* 89(B7), 5719. <https://doi.org/10.1029/JB089iB07p05719>

661 Richter, T., Sens-Schönfelder, C., Kind, R., Asch, G. 2014. Comprehensive observation and
662 modeling of earthquake and temperature-related seismic velocity changes in northern
663 Chile with passive image interferometry. *Journal of Geophysical Research: Solid Earth.*
664 119, 4747-4765, <https://doi.org/10.1002/2013JB010695>

665 Sato, H., Takahashi, H., Yamamoto, E., Fukuo, N., Uehara, M., Terasawa, Y. 1980.
666 Development of the crustal tilt observation method using borehole-type tiltmeters. *J.*
667 *Seismol. Soc. Japan.* 33(3), 343-368. https://doi.org/10.4294/zisin1948.33.3_343

668 Sawazaki, K., Kimura, H., Shiomi, K., Uchida, N., Takagi, R., Snieder, R. 2015. Depth-
669 dependence of seismic velocity change associated with the 2011 Tohoku earthquake,
670 Japan, revealed from repeating earthquake analysis and finite-difference wave
671 propagation simulation. *Geophys. J. Int.* 201(2), 741-763.
672 <https://doi.org/10.1093/gji/ggv014>

673 Schaff, D.P., Beroza, G.C. 2004. Coseismic and postseismic velocity changes measured by
674 repeating earthquakes. *J. Geophys. Res.* 109, B10302.
675 <https://doi.org/10.1029/2004JB003011>

676 Sens-Schönfelder, C., Wegler, U. 2006. Passive image interferometry and seasonal variations
677 of seismic velocities at Merapi Volcano, Indonesia. *Geophys. Res. Lett.* 33(21), L21302.
678 <https://doi.org/10.1029/2006GL027797>

679 Sens-Schönfelder, C., Wegler, U. 2011. Passive image interferometry for monitoring crustal
680 changes with ambient seismic noise. *Comptes Rendus Geoscience.* 343(8-9), 639-651.
681 <https://doi.org/10.1016/j.crte.2011.02.005>

682 Shapiro, N.M., Campillo, M., Kaminski, E., Vilotte, J.P., Jaupart, C. 2018. Low-frequency
683 earthquakes and pore pressure transients in subduction zones. *Geophys. Res. Lett.* 45,
684 11,083-11,094. <https://doi.org/10.1029/2018GL079893>

685 Shapiro, S.A., Huenges, E., Borm, G. 1997. Estimating the crust permeability from fluid-
686 injection-induced seismic emission at the KTB site. *Geophysical Journal International.*
687 131, F15-F18. <https://doi.org/10.1111/j.1365-246X.1997.tb01215.x>

688 Taira, T., Brenguier, F., Kong, Q. 2015. Ambient noise-based monitoring of seismic velocity
689 changes associated with the 2014 Mw 6.0 South Napa earthquake. *Geophys. Res. Lett.*
690 42(17), 6997-7004. <https://doi.org/10.1002/2015GL065308>

691 Takada, Y., Fukushima, Y. 2013. Volcanic subsidence triggered by the 2011 Tohoku
692 earthquake in Japan. *Nature Geoscience.* 6, 637-641. <https://doi.org/10.1038/ngeo1857>

693 Tokuda, T., Shimada, H. 2019. Classes of low-frequency earthquakes based on inter-time
694 distribution reveal a precursor event for the 2011 great Tohoku Earthquake. *Sci Rep.* 9,
695 9330. <https://doi.org/10.1038/s41598-019-45765-0>

696 Tsuji, T., Kawamura, K., Kanamatsu, T., Kasaya, T., Fujikura, K., Ito, Y., et al. 2013.
697 Extension of continental crust by anelastic deformation during the 2011 Tohoku-oki
698 earthquake: the role of extensional faulting in the generation of a great tsunami. *Earth*
699 *Planet. Sci. Lett.* 364, 44-58. <https://doi.org/10.1016/j.epsl.2012.12.038>

700 Uchide, T., Imanishi, K. 2018. Underestimation of microearthquake size by the magnitude
701 scale of the Japan Meteorological Agency: influence on earthquake statistics. *J. Geophys.*
702 *Res.: Solid Earth.* 123, 606-620. <https://doi.org/10.1002/2017JB014697>

703 Ueda, H., Fujita, E., Ukawa, M., Yamamoto, E., Irwan, M., Kimata, F. 2005. Magma
704 intrusion and discharge process at the initial stage of the 2000 activity of Miyakejima,
705 central Japan, inferred from tilt and GPS data. *Geophys. J. Int.* 161, 891-906.
706 <https://doi.org/10.1111/j.1365-246X.2005.02602.x>

707 Wang, Q.-Y., Brenguier, F., Campillo, M., Lecointre, A., Takeda, T., Aoki, Y. 2017.
708 Seasonal crustal seismic velocity changes throughout Japan. *J. Geophys. Res.: Solid*
709 *Earth*. 122, 7987-8002. <https://doi.org/10.1002/2017JB014307>

710 Wang, Q.-Y., Campillo, M., Brenguier, F., Lecointre, A., Takeda, T., Hashima, A. 2019.
711 Evidence of changes of seismic properties in the entire crust beneath Japan after the M_w
712 9.0, 2011 Tohoku-oki earthquake. *J. Geophys. Res.: Solid Earth*. 124, 8924-8941.
713 <https://doi.org/10.1029/2019JB017803>

714 Wegler, U., Nakahara, H., Sens-Schönfelder, C., Korn, M., Shiomi, K. 2009. Sudden drop of
715 seismic velocity after the 2004 M_w 6.6 mid-Niigata earthquake, Japan, observed with
716 passive image interferometry. *J. Geophys. Res.* 114(B6), B06305.
717 <https://doi.org/10.1029/2008JB005869>

718 Yoshida, K., Hasegawa, A., Yoshida, T. 2016. Temporal variation of frictional strength in an
719 earthquake swarm in NE Japan caused by fluid migration. *J. Geophys. Res.: Solid Earth*.
720 121, 5953-5965. <https://doi.org/10.1002/2016JB013022>

721 Yoshida, K., Hasegawa, A., Yoshida, T., Matsuzawa, T. 2019. Heterogeneities in stress and
722 strength in Tohoku and its relationship with earthquake sequences triggered by the 2011
723 M_9 Tohoku-Oki earthquake. *Pure Appl. Geophys.* 176, 1335-1355.
724 <https://doi.org/10.1007/s00024-018-2073-9>

725 Yoshida, K., Saito, T., Urata, Y., Asano, Y., Hasegawa, A. 2017. Temporal changes in stress
726 drop, frictional strength, and earthquake size distribution in the 2011 Yamagata-
727 Fukushima, NE Japan, earthquake swarm, caused by fluid migration. *J. Geophys. Res.:*
728 *Solid Earth*. 122, 10,379-10,397. <https://doi.org/10.1002/2017JB014334>

729 Yu, Z., Zhao, D., Niu, X., Li, J. 2018. Spatiotemporal distribution of low-frequency
730 earthquakes in southwest Japan: evidence for fluid migration and magmatic activity. *J.*
731 *Asian Earth Sci.* 151, 148-172. <https://doi.org/10.1016/j.jseaes.2017.10.033>